Globally and randomly coupled Ginzburg-Landau maps

Satoki Uchiyama* and Hirokazu Fujisaka†
Department of Physics, Kyushu University 33, Fukuoka 812-81, Japan
(Received 12 September 1996)

We propose a method for reducing a continuous dynamical system of coupled oscillators to discrete coupled maps. We apply the method to the coupled Ginzburg-Landau (GL) oscillators. In the case of global coupling, we find that the coupled GL maps exhibit irregular collective motions, and furthermore, we confirm numerically that the dynamical behavior is analogous to those of the original system. We obtain numerically the phase diagram in the case of random coupling, and propose a qualitative explanation by approximating the exponential function of the random coupling matrix along the lines of the spin glass theory. [S1063-651X(97)11707-X]

PACS number(s): 05.90.+m, 05.45.+b, 02.50.−r, 87.10.+e

I. INTRODUCTION

One of the frontiers of statistical physics is the investigation of open nonequilibrium systems where no detailed balance generally exists. These kinds of systems exhibit behaviors quite different from the equilibrium situation. The most significant aspect is the existence of self-sustained temporally oscillatory motion, which is totally distinct from the stochastic temporal evolution observed in the equilibrium state. Such an oscillatory behavior causes a lot of different phenomena in nature, e.g., dissipative structures, chaos, turbulence, and so on. In fact, many authors [1–3] believe that a large population of coupled oscillators can serve as a good model for studying these complex systems.

Recently, such oscillatory phenomena have been widely noticed also from a biological point of view. In particular in neuro-physiological experiments, limit cycle behavior of the activity of module of neurons have been reported [4–6], and these oscillations can be expected to be related with the brain functions. Thus, the collective dynamics of a system consisting of globally coupled identical elements is intensively studied in the area of modeling neural networks [7–17].

Some authors concentrate on systems whose dynamical element is described by the complex Ginzburg-Landau equation [8,9] (for the Ginzburg-Landau system with real coefficients, see [10]). In particular, the authors of Refs. [8] and [9] proposed a globally coupled Ginzburg-Landau oscillator system,

$$\dot{W}^{(j)}=(1+iC_0)W^{(j)}-(1+iC_2)|W^{(j)}|^2W^{(j)} + \frac{K}{N}(1+iC_1)\sum_{k=1}^{N}(W^{(k)}-W^{(j)}) \quad (j=1,\ldots,N), \tag{1.1}$$

where $W^{(j)}$ is the dynamical variable representing the state of the jth oscillator. N is the total number of oscillators, and the parameters C_0, C_1, C_2, and K are real. They found many types of attractors of Eq. (1.1), e.g., synchronized oscillation, clustering, collective chaos, and so on.

Furthermore, if the coupling coefficients are random [18–21], the system admits a multi-stable structure, which plays an interesting role.

Since we are aiming at both applications and mathematical tractable models, an alternative to rigorous analysis is to use the weak coupling limit among oscillator elements [1,22] (it is more successful in the case of random coupling [23,24]). The weak coupling approximation enables us to reduce the system to phase variables only, with the help of an adiabatic elimination of amplitudes. As is well known, the weak coupling approximation has been fruitfully applied in the analysis of the entrainment of a globally coupled phase oscillator system [11–15]. On the other hand, this reduction usually brings about the existence of a Liapunov function, which eventually leads to a fixed-point attractor. We will propose a reduced system that exhibits qualitatively the same dynamics as the nonreduced original differential equation system. From a technical point of view we will obtain our reduced dynamics by transforming the coupled differential equations to an equivalent coupled map system.

This paper is organized as follows. In Sec. II, we explain the general ideas for the reduction of a system of differential equations to a model discrete in time, and apply this approach to the Ginzburg-Landau oscillator system. In Sec. III, the dynamics of the discrete system is compared with that of the original differential equation for the case of global coupling. In Sec. IV, we discuss several types of attractors of the systems with the so-called (infinite-range) binary random coupling, i.e., a mixture of ferromagnetic and antiferromagnetic types of coupling. We obtain the phase diagram in terms of the coupling constant and the concentration of ferromagnetic bonds. A summary and a discussion on the advantage of our scheme for the construction of an oscillator network is briefly given in Sec. V.

II. COUPLED MAP SYSTEM

A. Construction of a coupled map system

Let us consider an oscillator described by a complex variable $W(t)$, which obeys an autonomous equation of motion,

$$\dot{W}(t)=\mathcal{F}(W(t),W^*(t)). \tag{2.1}$$

*Electronic address: uchiyama@daisy.phys.kyushu-u.ac.jp
†Electronic address: fuji3scp@mbox.nc.kyushu-u.ac.jp

Here $\mathcal{F}$ denotes a nonlinear function of W and W^*, which is assumed to possess a stable limit cycle. Since Eq. (2.1) is a two-dimensional, autonomous system, it apparently exhibits no chaotic behavior, but allows in principle for an analytical solution. By integrating Eq. (2.1) from t_n to $t_{n+1}(>t_n)$, t_n and t_{n+1} being arbitrary, we obtain the formal solution in terms of the initial value $W(t_n)$:

$$W(t_{n+1})=f_{t_{n+1}-t_n}(W(t_n),W^*(t_n)) \quad (t_{n+1}\geqslant t_n). \tag{2.2}$$

The transfer function $f_{t_{n+1}-t_n}$ satisfies both

$$W=f_0(W,W^*), \quad \partial f_{t-t_n}/\partial t|_{t=t_n}=\mathcal{F}(W(t_n),W^*(t_n)),$$

and the condition that any state suddenly settles onto the limit cycle by the transfer function f_∞. By putting $t_n=t_0+nT$, T being an arbitrary positive constant called the discrete time interval, Eq. (2.2) can be expressed in terms of the mapping system

$$W_{n+1}=f_T(W_n,W_n^*), \tag{2.3}$$

where $W_n\equiv W(t_n)$. We call Eq. (2.3) our element mapping system.

Now, we proceed to construct a coupled map system. In this paper we only consider linear couplings. Let $\mathcal{D}$ be a linear coupling operator defined by

$$\mathcal{D}W^{(j)}=\sum_{k=1}^{N}\hat{D}_{jk}W^{(k)} \quad (j=1,\ldots,N), \tag{2.4}$$

where $\hat{D}_{jk}$ denotes the elements of the constant matrix $\hat{D}$, and the superscript on W denotes the oscillator number. Note that $\mathcal{D}$ is not necessarily restricted to spatially local coupling. We are here concerned with the application to neural networks, where the connection among neurons may extend over the whole system. In this case all matrix elements of $\hat{D}$ can take nonvanishing finite values.

Our coupled map system is constituted by

$$W_{n+1}^{(j)}=\sum_{k=1}^{N}J_{jk}f_T(W_n^{(k)},W_n^{(k)*}) \quad (j=1,\ldots,N), \tag{2.5}$$

with the interaction

$$J_{jk}=(e^{T\hat{D}})_{jk}. \tag{2.6}$$

This construction is a straightforward extension of the method proposed in [25]. For a simple model, one can construct a coupled oscillator system that rigorously yields Eq. (2.5) [26]. Note that no restriction on the magnitude of T is imposed at present. It is easy to show that in the limit $T\to 0$, Eq. (2.5) reduces to the following coupled oscillator system:

$$\dot{W}^{(j)}=\mathcal{F}(W^{(j)},W^{(j)*})+\sum_{k}^{N}\hat{D}_{jk}W^{(k)} \quad (j=1,\ldots,N). \tag{2.7}$$

In this sense, the coupled map system (2.5) may be regarded as a generalization of coupled oscillators system (2.7) for any T value. Keeping $T\hat{D}_{jk}$ finite in the limit $T\to\infty$, on the other hand, we have the advantage that a dynamical variable $W_n^{(j)}$ obeying Eq. (2.5) can be described only by a phase variable that denotes the coordinate on the limit cycle of $\mathcal{F}$. Although this reduced equation has a structure similar to *coupled circle maps*, the full equation (2.5) can generally exhibit quite different dynamics. Our mapping system is expected to maintain the dynamical properties of the oscillators appropriately, while the reduction of degrees of freedom from $2N$ (phase + amplitude) to N (phase) makes the problem simple. This will be demonstrated in the following subsection.

Some remarkable features about Eq. (2.6) are listed below:

(1) Hermite coupling. If $\hat{D}$ is Hermitian, then J is also Hermitian. Namely,

$$\hat{D}_{jk}=\hat{D}_{kj}^*\Rightarrow J_{jk}=J_{kj}^*. \tag{2.8}$$

This is a precondition for the existence of a Liapunov function [27].

(2) In-phase (synchronization) condition. If $\hat{D}_{jk}$ satisfies the condition

$$\sum_{k=1}^{N}\hat{D}_{jk}=0 \quad (j=1,\ldots,N), \tag{2.9}$$

then the equality

$$\sum_{k=1}^{N}J_{jk}=1 \quad (j=1,\ldots,N) \tag{2.10}$$

holds. It guarantees the existence of the in-phase state, i.e., $W_n^{(1)}=W_n^{(2)}=\cdots=W_n^{(N)}=W_n$ where W_n is the limit cycle solution of the single map (2.3) (see Secs. III and IV), as a particular solution of Eq. (2.5).

(3) Difference coupling form. If $\hat{D}$ takes the form

$$\hat{D}_{jk}=D_{jk}-\delta_{jk}\sum_{l=1}^{N}D_{jl} \tag{2.11}$$

for a certain matrix D, Eq. (2.9) is satisfied. The form (2.11) will be referred to as the ''difference coupling form'' since

$$\sum_{k=1}^{N}\hat{D}_{jk}W^{(k)}=\sum_{k=1}^{N}D_{jk}(W^{(k)}-W^{(j)}) \quad (j=1,\ldots,N).$$

In the remaining part of the present paper, the coupling elements $\hat{D}_{jk}$ are chosen according to Eq. (2.11).

B. Coupled Ginzburg-Landau map system

Let us apply the above reduction scheme to the Ginzburg-Landau (GL) oscillator [8,9] given by

$$\mathcal{F}(W,W^*)=(1+iC_0)W-(1+iC_2)|W|^2W. \tag{2.12}$$

This equation is quite familiar in the study of chemical waves and spatiotemporal complex behaviors in reaction-

diffusion systems. One easily checks that the equation of motion (2.1) with Eq. (2.12) has a unique stable limit cycle $W(t)=e^{i(C_0-C_2)t}$. The transfer function is immediately obtained by integration of Eq. (2.1):

$$f_T(W,W^*)=e^{i(C_0-C_2)T}W[(1-e^{-2T})|W|^2 + e^{-2T}]^{-(1+iC_2)/2}. \quad (2.13)$$

The system has a symmetry with respect to a simultaneous phase shift (phase rotation symmetry). Then, without loss of generality, we can choose $C_0=C_2$, which implies a transformation to a rotating coordinate system with frequency C_0-C_2. For $T\to\infty$, Eq. (2.13) simplifies to

$$f_\infty(W,W^*)=W|W|^{-1-iC_2}. \quad (2.14)$$

Therefore, the coupled map system in the limit $T\to\infty$ is given by

$$W_{n+1}^{(j)}=\sum_{k=1}^{N} J_{jk}W_n^{(k)}|W_n^{(k)}|^{-1-iC_2} \quad (j=1,\ldots,N), \quad (2.15)$$

where the coupling J_{jk} remains finite by keeping $\hat{D}_{jk}T$ finite. Equations (2.14) and (2.15) will be called, respectively, the *GL map* and the *coupled GL map system*.

In order to extract the dynamics restricted on the limit cycle, let us introduce

$$W_n^{(j)}\equiv R_n^{(j)}e^{i\phi_n^{(j)}}, \quad e^{i\theta_n^{(j)}}\equiv f_\infty(W_n^{(j)},W_n^{(j)*}). \quad (2.16)$$

$R_n^{(j)}$ and $\phi_n^{(j)}$ are the amplitude and the phase of $W_n^{(j)}$, respectively, and $\theta_n^{(j)}$ is given by $\theta_n^{(j)}=\phi_n^{(j)}-C_2\ln R_n^{(j)}$. With this notation we obtain coupled equations for the phase variable $\theta_n^{(j)}$ only,

$$e^{i\theta_{n+1}^{(j)}}=\frac{\Sigma_k^N J_{jk}e^{i\theta_n^{(k)}}}{|\Sigma_k^N J_{jk}e^{i\theta_n^{(k)}}|^{1+iC_2}} \quad (j=1,\ldots,N). \quad (2.17)$$

The amplitude is determined by the phase dynamics as $R_{n+1}^{(j)}=|\Sigma_k^N J_{jk}e^{i\theta_n^{(k)}}|$, which implies a reduction of the number of degrees of freedom from $2N$ to N. This property makes the problem easier to handle and the numerical computation faster. Equation (2.17) is the fundamental equation of motion in the present paper for studying the dynamics in coupled oscillator systems. Note that the present phase model (2.17) reduces to coupled circle maps in a weak coupling case (see Appendix A).

It is worth stressing that Eq. (2.17) can be interpreted as a kind of neural network model. For simplicity consider $C_2=0$. If both the set of coupling elements J_{jk} and the initial values $e^{i\theta_0^{(j)}}$ are real, then, by putting $\sigma_n^{(j)}=e^{i\theta_n^{(j)}}(=\pm 1)$, Eq. (2.17) takes the following form:

$$\sigma_{n+1}^{(j)}=\mathrm{sgn}\left(\sum_{k=1}^{N} J_{jk}\sigma_n^{(k)}\right) \quad (j=1,\ldots,N). \quad (2.18)$$

This equation is identical to the well-known McCullock-Pitts model [28] with vanishing thresholds. As shown in Appendix B, it is possible to prove the existence of a Liapunov function of Eq. (2.17) decreasing monotonically in time, provided that the matrix J_{jk} is Hermitian.

III. GLOBALLY COUPLED GL MAP SYSTEM

In this section we consider the large population dynamics of GL oscillators with the global difference coupling form Eq. (2.11). The term ''global'' means that the coupling is all-to-all, and the coupling constants are defined by

$$D_{jk}=\frac{K}{N}(1+iC_1). \quad (3.1)$$

The corresponding oscillator system [the differential equation system (1.1)] with the global coupling has been studied by Hakim and Rappel [8] and Nakagawa and Kuramoto (NK) [9]. They determined the stability regions in the (C_1,C_2,K) space of two characteristic kinds of motion, the synchronized and the uniform phase distribution state. Furthermore the possibility of the existence of irregular motion in other parameter regions has been suggested.

Let E denote the unit matrix and I the matrix with all elements equal to unity. Then the matrix $\hat{D}$ is written as

$$\hat{D}=\frac{K}{N}(1+iC_1)(I-NE). \quad (3.2)$$

Hence we have

$$\hat{D}^m=(-1)^m K^m(1+iC_1)^m\hat{D} \quad (m=0,1,2,\ldots), \quad (3.3)$$

and the coupling matrix $J=\exp(T\hat{D})$ can be written as

$$J=E+\frac{\xi}{N}(I-NE), \quad \xi\equiv 1-e^{-(1+iC_1)KT}. \quad (3.4)$$

The diagonal and off-diagonal elements are thus given by

$$J_{jj}=1-\frac{(N-1)}{N}\xi\equiv J_{\mathrm{diag}}, \quad J_{jk}=\frac{\xi}{N}\equiv J_{\mathrm{off}} \quad (j\neq k). \quad (3.5)$$

In the limit $KT\to 0$ all off-diagonal elements vanish. One should note that the above expression always satisfies the synchronization condition (2.10). It is incidentally remarked that the globally coupled GL maps transfers a set of variables $W_n^{(j)}$ from a circle in the complex plane to another one (see Appendix C).

A. Linear stability of in-phase and uniform phase distribution states

Let us for a moment consider finite values of the discrete time step T. We will analyze the linear stability of particular solutions, and then compare the results with the the $T\to\infty$ limit and the $T\to 0$ limit. The limit $T\to 0$ will turn out to coincide with the corresponding differential equation system by NK. The following calculations are carried out with respect to variables $W_n^{(j)}$ instead of $\theta_n^{(j)}$.

First, let us consider the in-phase (IP) state, where all the oscillators are in-phase and the system behaves just like a single oscillator

$$W_n^{(j)}=1\equiv W_n^{\mathrm{IP}}. \tag{3.6}$$

Here the phase rotation symmetry permits the choice $W_0^{(j)}=1$. The linear stability of the solution (3.6) can be examined by solving the equations for the deviations $\delta W_n^{(j)}$ and $\delta W_n^{(j)*}$ from W_n^{IP}, i.e.,

$$\delta W_{n+1}^{(j)}=\sum_{k=1}^{N} J_{jk}\left(\left.\frac{\partial f_T}{\partial W}\right|_{W_n^{\mathrm{IP}}}\delta W_n^{(k)}+\left.\frac{\partial f_T}{\partial W^*}\right|_{W_n^{\mathrm{IP}}}\delta W_n^{(k)*}\right) \quad (j=1,\ldots,N), \tag{3.7}$$

and its complex conjugate. Instability occurs if the largest of the $2N$ eigenvalues becomes equal to unity in modulus (neutral condition). The eigenvalues of the stability matrix for the IP state can be classified into four types: $\lambda_1=1$ (1), $\lambda_2=e^{-2T}$ (1), λ_3 $(N-1)$, and λ_4 $(N-1)$, where the numbers in the parentheses refer to the degree of degeneracy. λ_3 and λ_4 are given by the characteristic equation $\lambda^2+\mathcal{A}\lambda+\mathcal{B}=0$, with the real coefficients

$$\mathcal{A}=(1+e^{-2T})\cos(C_1KT)-C_2(1-e^{-2T})\sin(C_1KT),$$

$$\mathcal{B}=e^{-2(K+1)T}.$$

λ_1 and λ_2 are irrelevant to the stability of the IP state. The neutral condition, $|\lambda_3|=1$ and $|\lambda_4|=1$, leads to

$$(\mathcal{A}^2+|\mathcal{A}^2-4\mathcal{B}|-4)^2=4\mathcal{A}^2|\mathcal{A}^2-4\mathcal{B}|. \tag{3.8}$$

It determines the stability boundary of the IP state for finite T. For $T\to 0$, Eq. (3.8) simplifies to

$$(1+C_1^2)K+2(1+C_1C_2)=0. \tag{3.9}$$

This condition agrees with that derived by NK for the differential equation system [9]. On the other hand, taking the limit $T\to\infty$ and keeping the product KT finite, the stability boundary is determined by

$$e^{2KT}-[\cos(C_1KT)-C_2\sin(C_1KT)]^2=0. \tag{3.10}$$

This result is specific for our model.

Second, let us consider the linear stability of the uniform phase distribution state (UPD). In this state the phase is uniformly distributed between 0 and 2π, $\theta^{(j)}=2\pi j/N$. The distribution function for the phase in the limit $N\to\infty$ is constant, $1/2\pi$. In contrast to the IP state we can say that the UPD state is the most disordered stationary state with respect to the phase distribution. The UPD solution is easily obtained as

$$W_n^{(j)}=\sqrt{\frac{e^{-2KT}-e^{-2T}}{1-e^{-2T}}}e^{i[-K(C_1-C_2)nT+\Theta j]}, \quad \Theta\equiv 2\pi/N. \tag{3.11}$$

This state exists only when the coupling strength obeys $K\leqslant 1$. The amplitude attains the value $\sqrt{1-K}$ in the limit $T\to 0$, in agreement with the corresponding differential equation system. With the help of cyclic determinant calculation [14], the eigenvalues of the stability matrix for the UPD state can be classified into six types: $\lambda_1=1$ $(N-2)$, $\lambda_2=e^{2(K-1)T}$ $(N-2)$, λ_3 (1), λ_4 (1), $\lambda_5(=\lambda_3^*)$ (1), and $\lambda_6(=\lambda_4^*)$ (1). λ_3 and λ_4 are given by a single characteristic equation $\lambda^2+\mathcal{A}\lambda+\mathcal{B}=0$, and λ_5 and λ_6 by $\lambda^2+\mathcal{A}^*\lambda+\mathcal{B}^*=0$, where the complex coefficients $\mathcal{A}$ and $\mathcal{B}$ are defined by

$$\mathcal{A}=\left(\frac{1+e^{2(K-1)T}}{2}\right)(1+e^{(1-iC_1)KT})-iC_2\left(\frac{1-e^{2(K-1)T}}{2}\right)(1-e^{(1-iC_1)KT}),$$

$$\mathcal{B}=e^{(3-iC_1)KT-2T}.$$

The eigenvalues λ_3, λ_4, λ_5, and λ_6 are relevant for the stability of the UPD state. Two neutral conditions for these four eigenvalues lead to

$$(|\mathcal{A}|^2+|\mathcal{A}^2-4\mathcal{B}|-4)^2=2\mathrm{Re}[\mathcal{A}^2(\mathcal{A}^{*2}-4\mathcal{B})]+2|\mathcal{A}|^2|\mathcal{A}^2-4\mathcal{B}|. \tag{3.12}$$

It is just the stability boundary of the UPD state for the finite T. To compare the stability boundary of the discrete equation with that of the differential one, we expand $\mathcal{A}$ and $\mathcal{B}$ with respect to T and obtain

$$K(K-1)[K(2K-1)C_1^2+4(K-1)(2K-1)C_1C_2-K(K-1)C_2^2+(3K-2)^2]=0 \tag{3.13}$$

in accordance with the analysis of the differential equation system [9]. Oppositely, taking the limit $T\to\infty$ by keeping KT finite, we obtain the equation that determines the boundary of the UPD state,

$$(1+C_2^2)(1+e^{2KT})+2[(1-C_2^2)\cos(C_1KT)+2C_2\sin(C_1KT)]e^{KT}=4. \tag{3.14}$$

This is an inherent result of the present model.

Equations (3.8) and (3.12) thus confirm that our system can cope with the differential system as the special case $T\to 0$. Note that K and T do not enter independently Eqs. (3.10) and (3.14), but appear in the product form KT. This fact shows that the limit $T\to\infty$ should be taken by keeping KT finite in order to get useful results.

The stable regions of the IP and the UPD state are shown in Fig. 1(a). The characteristic feature of these phase diagrams resembles that for the differential equation system [see Fig. 1(b)]. In particular, for $C_1=C_2=0$, Eqs. (3.10) and (3.14) both give $e^{KT}=1$. This implies that the motion in the globally coupled system with $C_1=C_2=0$ would be attracted to the IP or the UPD state depending on the sign of KT.

B. Numerical simulation

For the parameter values $C_1=-1$ and $C_2=2$, Eqs. (3.10) and (3.14) tell us that the IP and the UPD state lose their

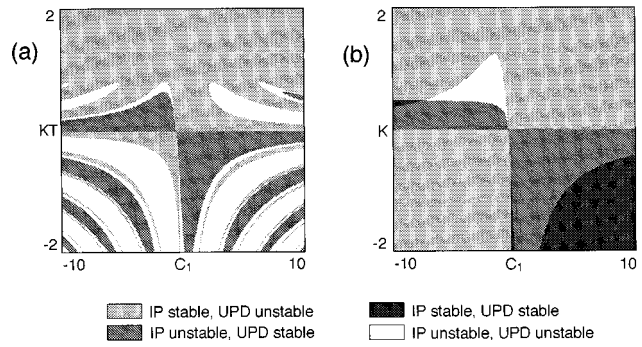

FIG. 1. Phase diagrams for coupled map system: (a) $T\to\infty$ with finite KT, $C_2=2.0$, (b) $T=0.01$, $C_2=2.0$. Note the difference of the scales of ordinates between the two figures. The phase diagram (b) is close to that for the differential equation system.

stability for $KT<0.73$ and $KT>0.56$, respectively. We numerically solved Eq. (2.17) with $N=100$, in order to confirm these predictions. Initial phases were set to be uniformly distributed between 0 and 2π. The numerical result shows that the IP state becomes unstable for $KT<1.0$. Such a discrepancy has also been reported in the differential equation system [9]. As mentioned by NK, it originates from the choice of the initial condition, which is not contained in the basin of the IP state for $0.73\leqslant KT<1.0$. Of course, if the system starts with an initial condition near the IP state, we find the stability boundary $KT=0.73$. On the other hand, the boundary of the UPD state agrees with the above mentioned value.

In order to observe attractors in the unstable regions of the IP and the UPD state, we numerically integrated Eq. (2.17) for $KT=0.56$, 0.62, 0.73, 0.90, 0.99, and 1.00. The oscillator number and the initial condition are the same as above. The time evolution of phases is shown in Fig. 2. This clearly shows that depending on KT the system has various attractors, i.e., (a) UPD, (b) *collective chaos*, (c) *cluster fusion*, (d) and (e) *cluster states*, (f) IP, which have been reported also by NK. Collective chaos implies a chaotic motion with N degrees of freedom, which emerges especially as a result of couplings among nonchaotic elements such as limit cycle oscillators. The dynamics of one site in the cluster fusion state reflects a repetition of the fusion to and the splitting from clusters. The dynamics in the n-cluster state is similar to the coupled n map system. Strictly speaking, (d) is the quasiperiodic 3-cluster state, and (c) the periodic 2-clusters state.

To study the trajectory instability of the attractors observed in Fig. 2, we investigate the Liapunov spectrum. From Eq. (2.17), the perturbation equation is written as

$$\delta\theta_{n+1}=G(n)\,\delta\theta_n, \tag{3.15}$$

where $\delta\theta_n=\mathrm{Col.}\,(\delta\theta_n^{(1)},\delta\theta_n^{(2)},\ldots,\delta\theta_n^{(N)})$ and

$$G_{jk}(n)\equiv(\mathrm{Re}-C_2\mathrm{Im})\left(\frac{J_{jk}e^{i\theta_n^{(k)}}}{\Sigma_l^N J_{jl}e^{i\theta_n^{(l)}}}\right). \tag{3.16}$$

The spectrum was obtained from the eigenvalues of the matrix U_n defined by $\delta\theta_n=U_n\delta\theta_0$ with $n=500$, after the transient has decayed. The results in Fig. 3 have characteristics similar to those found in NK. The spectra reflect the characteristics of the attractors observed in Fig. 2. Collective chaos ($KT=0.62$) has N positive Liapunov exponents, and cluster fusion ($KT=0.73$) has positive Liapunov exponents of order N. For the spectrum of quasiperiodic 3-clusters ($KT=0.90$) and periodic 2-clusters, the partitioning process into clusters depends on the initial condition. Thus, these spectra clearly manifest the band structure corresponding to their cluster partitions. The spectra for $KT=0.56$ and 1.00 have already been predicted analytically in the previous subsection.

The similarity of attractors between the differential equation system and the present mapping system is again emphasized. Although the present approach uses effective phase variables, we obtain quantitative coincidence with the differential coupled oscillator system, which involves both the phase and the amplitude variables. A similar striking coincidence cannot be achieved if coupled circle maps are employed.

IV. RANDOMLY COUPLED GL MAP SYSTEM

In this section, we consider the coupled GL map system with quenched random coupling D_{jk}. We will focus first on the construction of the coupling J, which is a remarkable feature of our model.

A. Binary random coupling $D_{jk}=\pm K/N$

For a simple realization of coupling D_{jk}, we adopt a binary randomness for each element D_{jk} along the lines of the $\pm J$ model in the spin glass theory, where the coupling is symmetric and either ferromagnetic $J(>0)$ with the probability p or antiferromagnetic $-J$ with $1-p$. Furthermore the coupling constants are assumed to be independent of each other, so that the distribution function factorizes for all elements. Namely, the probability distribution of D_{jk} is given by

$$P(D_{jk})=p\;\delta\left(D_{jk}-\frac{K}{N}\right)+(1-p)\,\delta\left(D_{jk}+\frac{K}{N}\right),\quad D_{jk}=D_{kj}, \tag{4.1}$$

where N, K, and p $(0\leqslant p\leqslant 1)$ denote the system size, the coupling strength, and the mixture rate with different signs of coupling, respectively. Without loss of generality, K is chosen to be positive since the coupling matrix is symmetric with respect to the transformation $(K,p)\to(-K,1-p)$. With Eq. (4.1) the nth moment of D_{jk} is easily obtained as

$$\langle D_{jk}^n\rangle=\left(\frac{K}{N}\right)^n[p+(-1)^n(1-p)]\equiv a_n. \tag{4.2}$$

Throughout this section, we focus on the influence of these parameters on the type of attractors.

In order to discuss the effect of random coupling on the statistical properties, we restrict the oscillator element to the simplest choice, $T\to\infty$ and $C_2=0$. As mentioned above, only the phase variable affects the system evolution in the $T\to\infty$ limit. In addition $C_2=0$ ensures the existence of a Liapunov function. However, the system has many different equilibria since frustration arises due to the mixture of positive and negative coupling constants. To get some impression about the complexity of the coupled system with

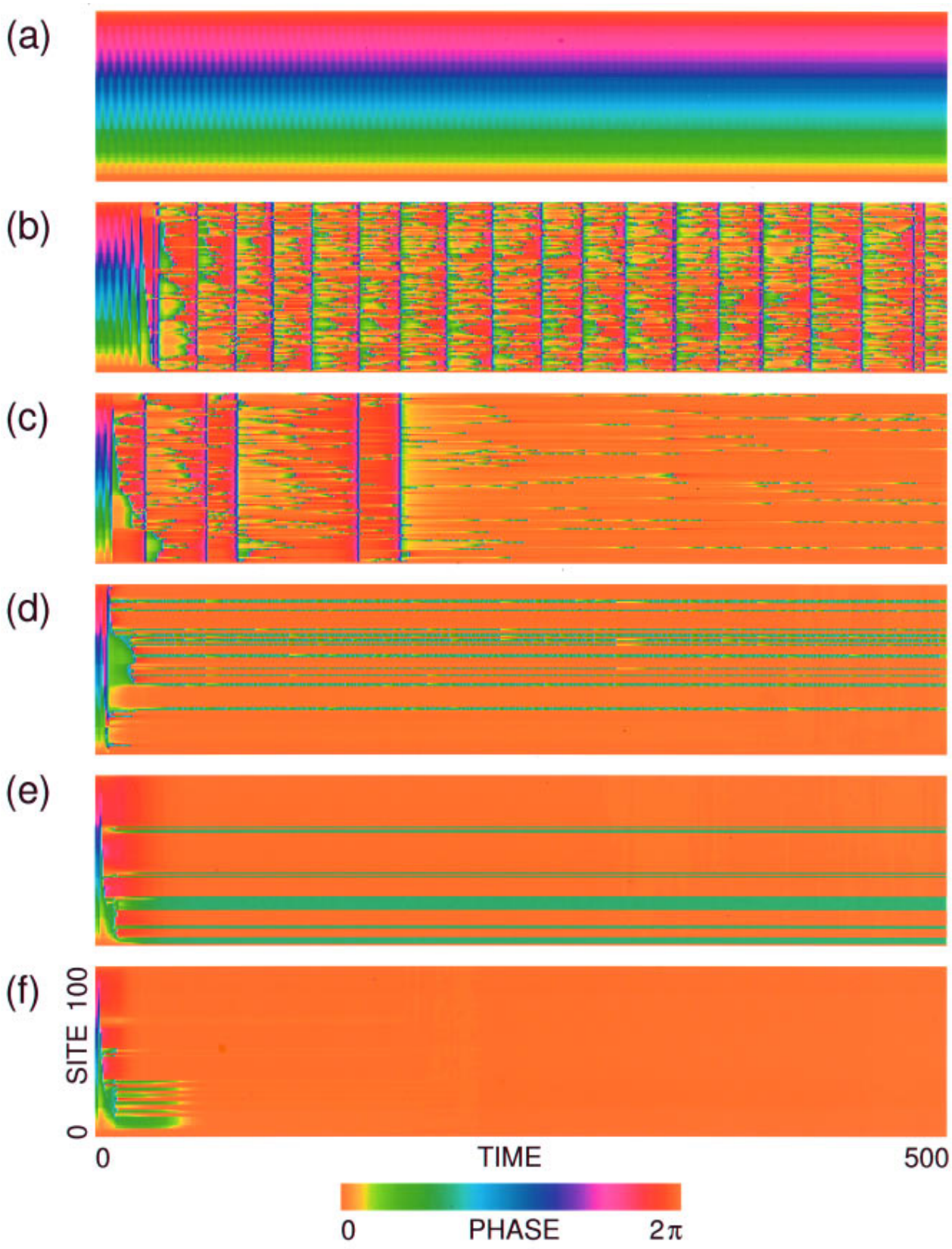

FIG. 2. (Color). Temporal evolutions of phase variables for Eq. (2.17) with $C_1 = -1.0$, $C_2 = 2.0$, and $N = 100$ for (a) $KT = 0.56$, (b) 0.62, (c) 0.73, (d) 0.90, (e) 0.99, and (f) 1.00. Phase values are expressed by the change of hue. For convenience, we put simultaneous phase variables on a vertical line although the global coupling imposes no spatial structure among the oscillators. Moreover, we set the color coordinate such that $\theta_n^{(1)}$ is fixed to zero at each time step.

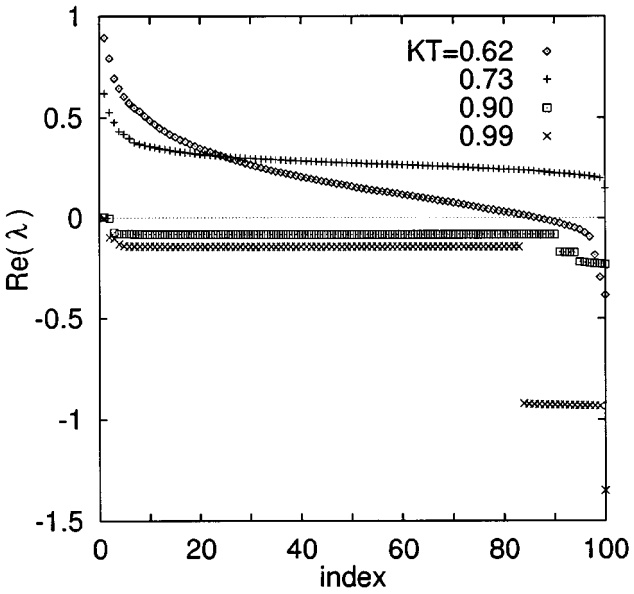

FIG. 3. Liapunov spectra for attractors observed in Fig. 2. The real part of the Liapunov exponents are arranged in order of magnitude.

quenched randomness, the exact calculation of the equilibrium states for small systems with $N=2,3$ is given in Appendix D.

Because of the above simplification, our Ginzburg-Landau oscillator system becomes equivalent to the XY spin system except the coupling form. We may apply the spin glass theory to our model to find equilibrium states in large systems. The theory of the Sherrigton-Kirkpatrick (SK) model [29] tells us that for randomly Gaussian distributed coupling constants J_{jk} (not D_{jk}) with finite first and second moment

$$\langle J_{jk}\rangle = J_0 \equiv \tilde{J}_0/N,\ \ \langle {J_{jk}}^2\rangle - \langle J_{jk}\rangle^2 = \sigma^2 \equiv \tilde{J}^2/N, \quad (4.3)$$

the phase diagram is determined by the parameter $\tilde{J}_0/\tilde{J}$ [30]. In the following we are mainly concerned with the moments of off-diagonal elements J_{jk}, $(j\neq k)$, since the diagonal part $\{J_{jj}\}$ is associated with the origin of the energy and never influences the equilibrium states.

It is difficult to calculate the functions $J_0=J_0(K,T,p,N)$ and $\sigma=\sigma(K,T,p,N)$ without approximations. Let the matrix J be approximated by the product of two matrices A and B according to $J\approx AB$, where

$$A_{jk}=[\exp(TD)]_{jk}, \quad (4.4)$$

$$B_{jk}=\exp\left(-T\ \delta_{jk}\sum_{l=1}^{N} D_{jl}\right). \quad (4.5)$$

This decomposition would hold rigorously, if A and B commute. But the jk matrix element of this commutation relation reads

$$\sum_l \left[D_{jl}\left(\delta_{lk}\sum_m D_{lm}\right)-\left(\delta_{jl}\sum_m D_{jm}\right)D_{lk}\right]$$

$$=D_{jk}\sum_{m=1}^{N}(D_{km}-D_{jm}), \quad (4.6)$$

and does not vanish in general. However, the average of Eq. (4.6) over random realization D vanishes, and its variance is estimated as $O(N^{-3/2})$ by means of the random walk theory [31]. So, the above decomposition holds asymptotically in the limit $N\to\infty$.

Furthermore, if we neglect the correlation between the two matrices, then $\langle J\rangle$ is replaced by the product of the average values,

$$\langle J\rangle \approx \langle A\rangle\langle B\rangle. \quad (4.7)$$

Although the validity of the decoupling approximation is not obvious, we will confirm in the following that this approximation yields qualitatively quite good results for the parameter region of interest.

B. Moments of J_{jk}

To calculate the moments of the elements of random matrices A and B, we make an approximation described in Appendix E. The results are

$$\langle A_{jk}\rangle = \frac{1}{N}(e^{KT(2p-1)}-1)+O(N^{-2}), \quad (4.8a)$$

$$\langle A_{jj}\rangle = 1+\frac{1}{N}(e^{KT(2p-1)}-1)+\frac{(KT)^2}{N}2p(1-p)+O(N^{-2}), \quad (4.8b)$$

$$\langle A_{jk}^2\rangle = \frac{1}{N^2}(e^{KT(2p-1)}-1)^2+\left(\frac{KT}{N}\right)^2 4p(1-p)+O(N^{-3}), \quad (4.8c)$$

$$\langle A_{jk}^3\rangle = \frac{1}{N^3}(e^{KT(2p-1)}-1)^3+\left(\frac{KT}{N}\right)^3 4p(1-p)(2p-1)+O(N^{-4}), \quad (4.8d)$$

and

$$\langle B_{jj}^m\rangle = e^{-mKT(2p-1)}+O(N^{-1}) \quad (m\geqslant 1), \quad (4.9)$$

where $j\neq k$. By using Eqs. (4.8) and (4.9), the moments of the off-diagonal elements J_{jk} are evaluated as follows:

$$\langle J_{jk}\rangle = \frac{1}{N}(1-e^{-KT(2p-1)}), \quad (4.10a)$$

$$\langle J_{jk}^2\rangle = \frac{1}{N^2}(1-e^{-KT(2p-1)})^2+\left(\frac{KT}{N}\right)^2 4p(1-p)e^{-2KT(2p-1)}, \quad (4.10b)$$

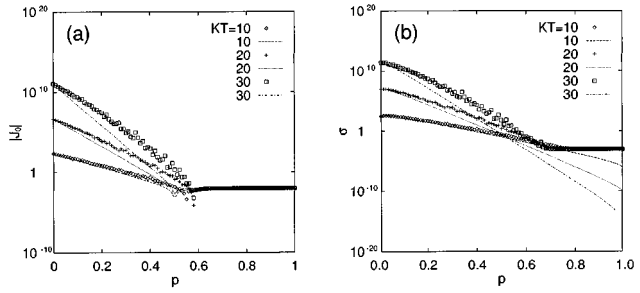

FIG. 4. The mean and variance of off-diagonal elements J_{jk} for the random coupling case. Symbols are numerical results and lines stand for approximate results (4.10a) and (4.11). For details, see the text.

$$\langle J_{jk}^3\rangle=\frac{1}{N^3}(1-e^{-KT(2p-1)})^3 + \left(\frac{KT}{N}\right)^3 4p(1-p)(2p-1)e^{-3KT(2p-1)}, \tag{4.10c}$$

and so on. One easily finds that the distribution of J_{jk} is not Gaussian for small N, and that it approaches a delta function with a peak at zero for $N\to\infty$. Furthermore, $\langle J_{jk}^2\rangle-\langle J_{jk}\rangle^2$ is of the order $O(N^{-2})$ though it should be $O(N^{-1})$ [see Eq. (4.3)]. Concerning the spin glass theory, this difference implies that the term proportional to $\langle J_{jk}\rangle$ in the mean field treatment could hide the term proportional to $\langle J_{jk}^2\rangle$ if we take the thermodynamic limit. In this sense, only for intermediate values of N an approximately Gaussian distribution may be realized.

By making use of the above results, the standard deviation $\sigma=\sqrt{\langle J_{jk}^2\rangle-\langle J_{jk}\rangle^2}$ is obtained as

$$\sigma=\frac{KT}{N}2\sqrt{p(1-p)}e^{-KT(2p-1)}. \tag{4.11}$$

σ vanishes for $p=0$ or $p=1$ in accordance with the global ferromagnetic and the anti-ferromagnetic coupling, respectively. In a similar way the diagonal part $\langle J_{jj}\rangle$ is obtained as

$$\langle J_{jj}\rangle=1-\frac{N-1}{N}(1-e^{-KT(2p-1)}) + \frac{(KT)^2}{N}2p(1-p)e^{-KT(2p-1)}. \tag{4.12}$$

By combining $\langle J_{jj}\rangle$ with $\langle J_{jk}\rangle$, the synchronization condition (2.10) is confirmed in the thermodynamic limit even in the random coupling case. Needless to say, these mean values coincide with the corresponding values in the global coupling cases for $p=0$ and 1.

In order to verify the analytical estimates, we carried out numerical simulations. For that purpose we generated a random matrix D_{jk} for several parameters in the range $0<KT\leqslant 50$ and $0\leqslant p\leqslant 1$, and investigated the moments $\langle J_{jk}\rangle$ and $\langle J_{jk}^2\rangle$ with 9900 $(=N^2-N)$ off-diagonal matrix elements. The results are plotted in Fig. 4. The analytical estimates seem to be in overall agreement with the numerical results.

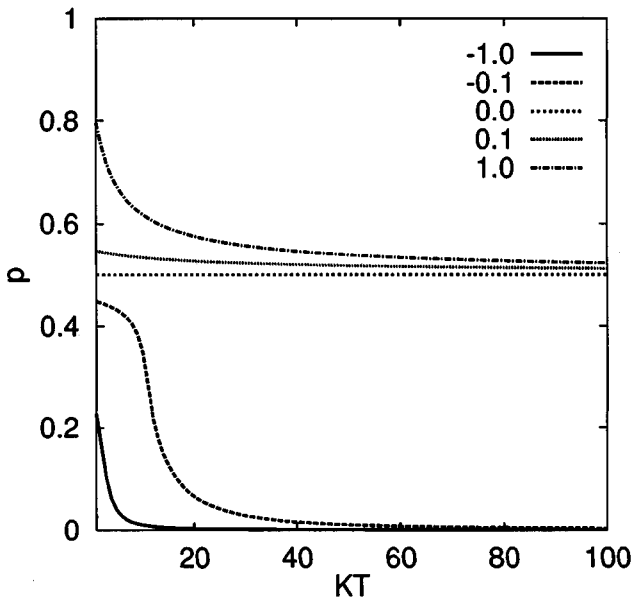

FIG. 5. Contours corresponding to $\tilde{J}_0/\tilde{J}=\text{const}$ in the (KT,p) plane. Numerical values are const$\times N^{-1/2}$.

C. Candidate for phase boundaries

We assume that the curves $\tilde{J}_0/\tilde{J}=\text{const}$ must be a phase boundary for certain values of the constant. Namely, by noting the results of the SK model, the following expression shall serve as a phase boundary in the (KT,p) plane:

$$\frac{(1-e^{-KT(2p-1)})}{2KT\sqrt{p(1-p)}e^{-KT(2p-1)}}=\text{const}\times N^{-1/2}. \tag{4.13}$$

Figure 5 depicts these curves for several values of the right-hand side of Eq. (4.13). Although we have no theory at hand to determine the constant, phases would be separated by these contours.

We numerically simulated the dynamics of our model with different realization of D_{jk}, and investigated what kinds of attractors are realized depending on the parameter values $0\leqslant p\leqslant 1$ and $0<KT\leqslant 50$. For the simulations we used the system size $N=50$ and 100, and 100 runs each time. To observe dynamical behavior and to evaluate the attractors quantitatively, we introduce two complex order parameters by

$$Z_1=\frac{1}{N}\sum_{j=1}^{N}\exp(i\theta_n^{(j)}),\quad Z_2=\frac{1}{N}\sum_{j=1}^{N}\exp(2i\theta_n^{(j)}), \tag{4.14}$$

where $0\leqslant|Z_1|\leqslant 1,0\leqslant|Z_2|\leqslant 1$. Note that only their amplitudes are relevant because of the phase rotation symmetry. The order parameter Z_1 characterizes the distance to the in-phase state, and Z_2 the distance to a two cluster state with phase difference π. In particular, $|Z_1|=|Z_2|=1$ stands for the IP state, and $|Z_1|=0$ and $|Z_2|=1$ for the two cluster state with equal domain size.

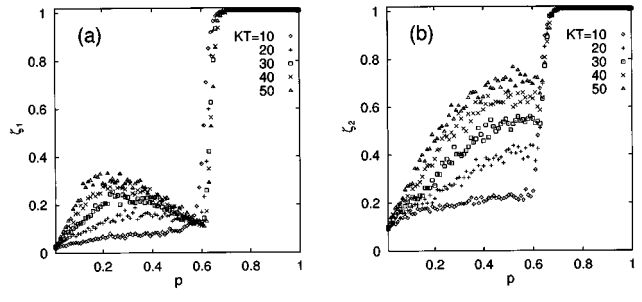

FIG. 6. Numerical results for order parameters: (a) ζ_1 vs p, (b) ζ_2 vs p. The system size and the number of ensembles are fixed to 100 and 100, respectively. The data are also used in Fig. 7.

Figure 6 shows the dependence of the quantities $\zeta_1 \equiv \langle |Z_1| \rangle$ and $\zeta_2 \equiv \langle |Z_2| \rangle$ on both KT and p. Here the angular brackets represent an average with respect to both the initial conditions of phase variables and the realization of the random matrix D_{jk}. These figures suggest the existence of three phases: (1) *in-phase* state characterized by $(\zeta_1, \zeta_2) \simeq (1,1)$, (2) *antiphase* state (AP) characterized by $(\zeta_1, \zeta_2) \simeq (0,1)$, and (3) *oscillator glass* state (OG) characterized by $(\zeta_1, \zeta_2) \simeq (0,0)$ [32]. Figure 7 depicts the numerically obtained phase diagram. For convenience we present numerical values for the phase boundaries

$$\zeta_1 = 0.94 \pm 0.05, \text{IP-AP}; \quad \zeta_2 = 0.25 \pm 0.01, \text{AP-OG}. \tag{4.15}$$

A concrete discussion of each phase is summarized below.

(1) In-phase state: Our analysis presented above already suggests that in the IP state the majority of the coupling coefficients J is positive. Hence the occurrence of the IP state for large values of p is easily understood. It seems plausible that in the limit $KT \to 0$, where the extremely long relaxation time prevents us from approaching equilibrium,

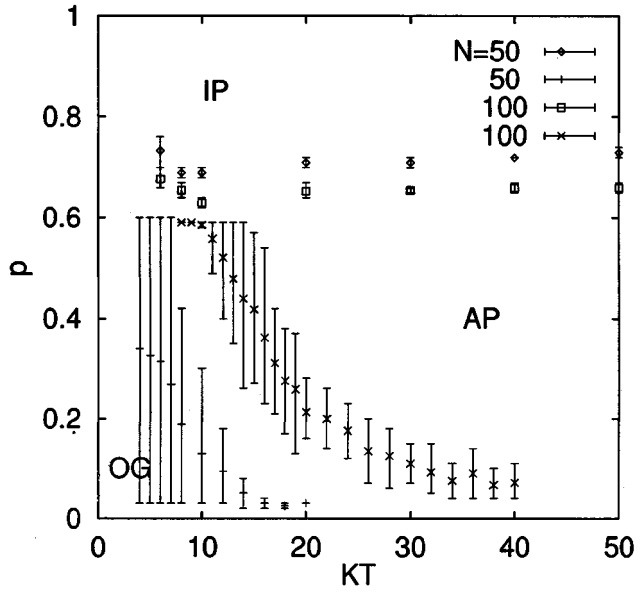

FIG. 7. Numerically determined phase diagram using the definition (4.15). The bars indicate the transition region in p. The system size plays a crucial role on the position of phase boundaries. It is explicitly involved in Eq. (4.13). Compare with Fig. 5.

the IP-AP boundary tends to the point $(KT,p) = (0,1)$. On the contrary, in the limit $KT \to \infty$, Fig. 7 suggests that the boundary between IP and AP asymptotically approaches a constant value in accordance with our analytic prediction. In ordinary spin glass theory the phase transition line corresponds to the choice const$=1$ in Eq. (4.13). In the present case, our numerical result suggests a value different from unity. The reason may be attributed to the approximate results (4.10a) and (4.10b), which were derived under the assumption of nonvanishing $\langle D_{jk} \rangle$. The IP-AP transition line unfortunately lies close to $p = 0.5$ where our ansatz breaks down.

(2) Anti-phase state: In this state, the phase distribution has two broad peaks separated by π. As p is decreased, ζ_2 decreases from about unity to zero. The AP-OG transition line shown in Fig. 7 is reproduced quite convincingly by inserting a negative value for the constant (see Fig. 5).

(3) Oscillator glass state: This state is similar to the UPD state $(\zeta_1 = 0, \zeta_2 = 0)$ in the sense that ζ_1 andζ_2 vanish approximately. We did not observe an OG state with ζ_1 and ζ_2 equal to zero. Such a feature is related to the existence of a Liapunov function for $C_2 = 0$ [33]. Instead, we found a small region where both $\zeta_1 \ll 1$ and $\zeta_2 \ll 1$ hold. Numerical simulations generate this so-called oscillator glass state for the corresponding parameter values (Fig. 6). The majority of coupling elements belongs to negative values, which is similar to the fact that the UPD state is stable in the case of global anti-ferromagnetic coupling [Eq.(3.14)].

For a finite N, the AP state can be observed in the parameter region where $\langle J_{jk} \rangle \cong 0$, and the numerically obtained candidate for AP-OG boundary resembles the curve defined by Eq. (4.15). But, its existence is not proved by the SK theory and our discussion. When N tends to infinity, the curves given by Eq. (4.13) with positive values for the constant tend to the line $p = 0.5$ from above, whereas the curves with negative values for the constant approach $p = 0.5$ from below for any value of KT. As a consequence the AP phase would vanish (see Fig. 7) in the thermodynamic limit.

Let us emphasize the similarity between Fig. 7 and the phase diagram in the SK XY spin system. References [34,35] reported on two mixed phases, which may have the aspect of both the ferromagnetic phase and the spin glass one. These two were separated by three boundaries, i.e., $\tilde{J}_0/\tilde{J} = 1$, the de Almeida–Thouless line and the Gabay-Toulouse line [36]. However, returning to our phase diagram, it is still difficult to recognize whether critical values different from $\tilde{J}_0/\tilde{J} \sim 1$ exist at all. In such a case a theoretical or numerical determination would be tempting. Consequently we have yet no definite idea about the relation between the mixed states in the SK XY spin system and the AP phase in the present system except that both are surrounded by the most ordered phase (IP, ferromagnetic) and the most disordered one (OG, spin glass) in each phase diagram.

V. CONCLUDING REMARKS

In this paper, we proposed a general approach to constructing coupled map systems for coupled differential equations and applied it to the coupled GL oscillator system. The limit $T \to \infty$ is of our particular interest. For global coupling

theoretical and numerical results coincide with the full differential equation system. In this sense, as long as global coupling is concerned, the GL map system well describes the GL equation system in contrast to the frequently investigated circle map system [16,17]. Our success is even more striking if one keeps in mind that each oscillator is completely described by phase variables at every discrete time step. For random coupling matrices we constructed quantitatively the phase diagram with the help of the spin glass theory. An extension to different random realizations, e.g., $\langle D_{jk}\rangle \neq 0$, is straightforward.

Finally, we add a comment on the relation between the present model and some neural network models. Our model with $C_2=0$ and $T\to\infty$ belongs to the group of phaser (oscillator) neural network models [23,24,37,38]. J is specified by the *generalized Hebb rule*, which is designed to retrieve embedded phase patterns. In this case, C_1 becomes unimportant for the lack of a unique phase direction for random couplings. Replica symmetry solutions for the model reveal the storage capacity $\alpha_c=0.0377$. In the future, we intend to generalize this network to $C_2\neq 0$ for which no Liapunov function is available and interesting dynamical behaviors are expected to occur even in a rotating frame. Research in this direction is now in progress, and will be reported elsewhere.

ACKNOWLEDGMENTS

The authors thank W. Just for a critical reading of the manuscript. This study was partially supported by Grant-in-Aid for General Scientific Research (No. 40156849) from the Ministry of Education and Culture, Japan.

APPENDIX A: WEAK COUPLING LIMIT OF THE COUPLED GL MAP SYSTEM

Equation (2.17) is rewritten as

$$\theta_{n+1}^{(j)}=\theta_n^{(j)}+\alpha_{jj}+\arg(h_n^{(j)})-C_2\ln|h_n^{(j)}|,$$

$$h_n^{(j)}=\sum_{k=1}^{N}|J_{jk}|e^{i(\theta_n^{(k)}-\theta_n^{(j)}+\alpha_{jk}-\alpha_{jj})}, \tag{A1}$$

where we put $J_{jk}=|J_{jk}|e^{i\alpha_{jk}}$. α_{jj} stands for the intrinsic frequency of the jth oscillator. In the weak coupling case ($\beta_{jk}\equiv|J_{jk}|/|J_{jj}|\ll 1$ for $k\neq j$), Eq. (A1) reduces to

$$\theta_{n+1}^{(j)}=\theta_n^{(j)}+\alpha_{jj}-C_2\ln|J_{jj}|+\sqrt{1+C_2^2}\sum_{k=1}^{N}\beta_{jk}\sin(\theta_n^{(k)}-\theta_n^{(j)}+\alpha_{jk}-\alpha_{jj}-\arctan C_2), \tag{A2}$$

in the lowest order with respect to the relative coupling strength β_{jk}. This type of phase model is called coupled circle maps, and has been used by several authors [16–18] to study synchronized oscillations and the dynamical behavior associated with its breakdown.

APPENDIX B: LIAPUNOV FUNCTION FOR $C_2=0$

If the matrix J is Hermitian, the equation of motion (2.17) for $C_2=0$ has the Liapunov function

$$E_n=-\frac{1}{2}\sum_{j,k}^{N}J_{jk}e^{-i\theta_n^{(j)}}e^{i\theta_n^{(k)}}. \tag{B1}$$

This is proved as follows. First, note that E_n is a real function since J is Hermitian. We define the local potential $h_n^{(j)}=\Sigma_{k=1}^{N}J_{jk}e^{i\theta_n^{(k)}}$. The energy change $\Delta E_n\equiv E_{n+1}-E_n$ with the change at the site j is calculated as

$$\Delta E_n=-|h_n^{(j)}|[1-\cos(\arg h_n^{(j)}-\theta_n^{(j)})]\leqslant 0. \tag{B2}$$

Since E_n monotonically decreases in the course of time, it has the property of a Liapunov function.

APPENDIX C: GEOMETRIC INTERPRETATION OF GLOBALLY COUPLED GL MAPS

The time evolution of amplitude $R_n^{(j)}$ can be read off from Eq. (2.15) as

$$R_n^{(j)}=\left|\sum_{k=1}^{N}J_{jk}e^{i\theta_n^{(k)}}\right|=\left|J_{\rm off}\sum_{k=1}^{N}e^{i\theta_n^{(k)}}+(J_{\rm diag}-J_{\rm off})e^{i\theta_n^{(j)}}\right|.$$

This expression indicates that the set $\{W_n^{(j)}:j=1,\ldots,N\}$ is transfered from the locations on a circle in the complex W space with the center $J_{\rm off}\Sigma e^{i\theta_n^{(k)}}$ and the radius $|J_{\rm diag}-J_{\rm off}|=e^{-KT}$ to one with the center $J_{\rm off}\Sigma e^{i\theta_{n+1}^{(k)}}$ and the same radius.

APPENDIX D: EQUILIBRIA CONSTRUCTED FOR $N=2,3$ GL MAPS

In this Appendix we analyze the systems of two and three coupled elements with $C_2=0$ and symmetric couplings $D_{jk}=D_{kj}$. The condition $C_2=0$ prevents our system from permanent temporal evolution. As defined in Sec. IV, we will adopt a binary coupling strength

$$D_{jk}=\pm K/N. \tag{D1}$$

1. $N=2$ case

Since only one coupling (D_{12}) between the two oscillators occurs, Eq. (2.11) gives a unique coupling configuration, regardless of the sign of self-couplings, as

$$\hat{D}=\frac{K}{2}\begin{pmatrix}-1 & 1\\ 1 & -1\end{pmatrix}, \tag{D2}$$

where $K>0$ (<0) means the ferromagnetic (antiferromagnetic) case using the terminology of spin systems. The coupling matrix $J=e^{T\hat{D}}$ can be easily obtained as

$$J=\frac{1}{2}\begin{pmatrix}1+e^{-KT} & 1-e^{-KT}\\ 1-e^{-KT} & 1+e^{-KT}\end{pmatrix}. \tag{D3}$$

The equilibrium state (θ_1^0,θ_2^0) of Eq. (2.17) is determined by

TABLE I. Equilibrium states and their stability for $N=3$. We use an abbreviation $\gamma \equiv g(KT)$, where $g(x)$ is given by Eq. (D7). Stars refer to the solutions whose existence condition depends on KT. We give no explicit existence condition because all of them are unstable.

	$(\theta_2^0-\theta_1^0 \bmod 2\pi, \theta_3^0-\theta_1^0 \bmod 2\pi)$	
(D_{12},D_{23},D_{31})	Stable	Unstable
$(+,+,+)$	(0,0)	$(\pi,0)^\star$, $(0,\pi)^\star$, $(\pi,\pi)^\star$, $(\frac{2}{3}\pi,-\frac{2}{3}\pi)$, $(-\frac{2}{3}\pi,\frac{2}{3}\pi)$
$(+,-,+)$	$(\gamma,-\gamma)$, $(-\gamma,\gamma)$	$(\pi,0)$, $(0,\pi)$, $(\pi,\pi)^\star$, (0,0)
$(-,+,-)$	(π,π)	$(\pi,0)^\star$, $(0,\pi)^\star$, (0,0), $(\gamma,-\gamma)$, $(-\gamma,\gamma)$
$(-,-,-)$	$(\frac{2}{3}\pi,-\frac{2}{3}\pi)$, $(-\frac{2}{3}\pi,\frac{2}{3}\pi)$	$(\pi,0)$, $(0,\pi)$, (π,π), (0,0)

$$e^{i\theta_1^0}=\frac{J_{11}e^{i\theta_1^0}+J_{12}e^{i\theta_2^0}}{\left|J_{11}e^{i\theta_1^0}+J_{12}e^{i\theta_2^0}\right|}, \quad e^{i\theta_2^0}=\frac{J_{21}e^{i\theta_1^0}+J_{22}e^{i\theta_2^0}}{\left|J_{22}e^{i\theta_1^0}+J_{22}e^{i\theta_2^0}\right|}. \tag{D4}$$

This set of equations has two types of solutions $\theta_1^0-\theta_2^0=0$ and π. The linear stability analysis shows that $\theta_1^0-\theta_2^0=0$ and π are stable for $K>0$ and $K<0$, respectively.

2. $N=3$ case

For $N=3$, the calculation of J goes along the lines of the previous section. Note however, that two different coupling configurations occur: all of three couplings are either ferromagnetic, i.e., $(D_{12},D_{23},D_{31})=(+,+,+)$ or antiferromagnetic, $(-,-,-)$ (type 1) and one of them has a different sign from the others, namely, $(+,+,-)$,$(+,-,-)$,$(+,-,+)$,$(-,+,+)$,$(-,+,-)$, and $(-,-,+)$ (type 2).

For type 1, matrices $\hat{D}$ and J are given by

$$\hat{D}=\frac{K}{3}\begin{pmatrix} -2 & 1 & 1 \\ 1 & -2 & 1 \\ 1 & 1 & -2 \end{pmatrix},$$

$$J=E+\frac{1-e^{-KT}}{3}\begin{pmatrix} -2 & 1 & 1 \\ 1 & -2 & 1 \\ 1 & 1 & -2 \end{pmatrix}, \tag{D5}$$

where E is the 3×3 unit matrix. This coupling corresponds to the $(+,+,+)$ coupling for $K>0$ and to $(-,-,-)$ for $K<0$. For type 2, by taking into account the permutation symmetry, it is sufficient to define matrices $\hat{D}$ and J by

$$\hat{D}=\frac{K}{3}\begin{pmatrix} 0 & 1 & -1 \\ 1 & -2 & 1 \\ -1 & 1 & 0 \end{pmatrix},$$

$$J=\frac{1}{3}E+\frac{1}{6}\begin{pmatrix} q+3q^{-1/3} & -2q & q-3q^{-1/3} \\ -2q & 4q & -2q \\ q-3q^{-1/3} & -2q & q+3q^{-1/3} \end{pmatrix}, \tag{D6}$$

where $q\equiv e^{-KT}$. This representation corresponds to $(+,-,+)$ for $K>0$ and to $(-,+,-)$ for $K<0$. We recall that the signs of the diagonal elements of D are unimportant.

With these J's, it is sufficient to solve two kinds of coupled algebraic equations for the fixed point $(\theta_2^0-\theta_1^0, \theta_3^0-\theta_1^0)$. Note that it is possible to choose $\theta_1^0=0$ without loss of generality because of the rotational symmetry. The equilibrium states for $N=3$ are summarized in Table I with the results of their linear stability. The solution for the $(+,-,+)$ configuration depends on KT through the function $g(KT)$, defined by

$$g(x)=\arccos\left(\frac{-1+e^{-x}}{2-3e^{x/3}+e^{-x}}\right). \tag{D7}$$

We remark that (see Fig. 8) $g(+\infty)=\pi/2$, $g(0)=\pi/3$, $g(-\infty)=0$.

We briefly discuss the relation between the three GL map system and the spin system made of three XY spins [39] with three bonds $J_{jk}=\pm J$. The phase of the GL map with $C_2=0$ corresponds to the direction of XY spin. The difference with respect to equilibria and stability is observed in the coupling strength dependence. Such dependence is enhanced with the system size.

APPENDIX E: MOMENTS OF A_{jk} AND B_{jk}

First of all, we consider the average of the matrix element A_{jk}. To this end we illustrate our approach on the simpler

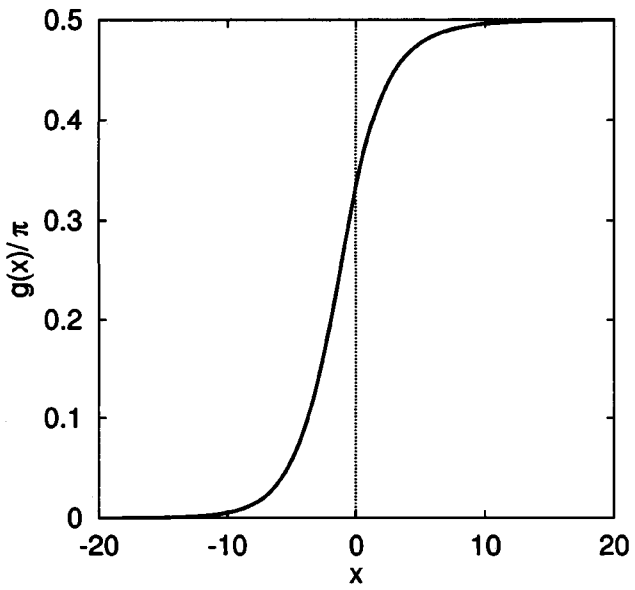

FIG. 8. The function $g(x)$, [Eq. (D7)]. It determines the formation of stable solutions for $(+,-,+)$.

case $N=2$. The off-diagonal element A_{12} is expanded up to T^5 as

$$A_{12}=TD_{12}+\frac{1}{2!}T^2(D_{11}D_{12}+D_{12}D_{22})+\frac{1}{3!}T^3(D_{11}^2D_{12}+D_{12}^3 + D_{11}D_{12}D_{22}+D_{12}D_{22}^2)+\frac{1}{4!}T^4(D_{11}^3D_{12}+2D_{11}D_{12}^3 + D_{11}^2D_{12}D_{22}+2D_{12}^3D_{22}+D_{11}D_{12}D_{22}^2+D_{12}D_{22}^3) + \frac{1}{5!}T^5(D_{11}^4D_{12}+3D_{11}^2D_{12}^3+D_{12}^5+D_{11}^3D_{12}D_{22} + 4D_{11}D_{12}^3D_{22}+D_{11}^2D_{12}D_{22}^2+3D_{12}^3D_{22}^2+D_{11}D_{12}D_{22}^3 + D_{12}D_{22}^4)+O(T^6).$$

Taking the average over random variables D_{jk} and noting that $\langle D_{11}^l D_{12}^m D_{22}^n\rangle = a_l a_m a_n$, and so on, we obtain

$$\langle A_{jk}\rangle = Ta_1+\frac{1}{2!}T^2 2a_1^2+\frac{1}{3!}T^3(a_3+2a_2a_1+a_1^3) + \frac{1}{4!}T^4(6a_3a_1+2a_2a_1^2)+\frac{1}{5!}T^5(a_5+2a_4a_1 + 6a_3a_2+6a_3a_1^2+a_2^2a_1)+O(T^6),$$

where the index 12 is replaced by jk only to denote the averaged off-diagonal element.

By carrying out a same procedure, the calculation for arbitrary N is straightforward, and yields

$$\langle A_{jk}\rangle = Ta_1+\frac{1}{2!}T^2Na_1^2 + \frac{1}{3!}T^3[(N-1)^2a_1^3+2(N-1)a_2a_1+a_3] + \frac{1}{4!}T^4[(N-2)(N^2-N-3)a_1^4+2(N+1)a_3a_1 + (3N^2-N-8)a_2a_1^2] + \frac{1}{5!}T^5[(N-2)(N^3-2N^2-4N+4)a_1^5 + (4N^2-5)(N-2)a_2a_1^3+(5N^2-11N+3)a_2^2a_1 + (3N^2-2N-2)a_3a_1^2+2(2N-1)a_3a_2 + 2(N-1)a_4a_1+a_5]+O(T^6).$$

In the thermodynamic limit $N\to\infty$, by neglecting $O(N^{-2})$ terms, the general term of the expression turns out to be $N^{-1}(TNa_1)^n n!$, $(n=1,\ldots,5)$, where we used $a_1=O(N^{-1})$. Inductively assuming that this holds in general, and summing up the series, we obtain Eq. (4.8a). It is noted that K and T always appear within the product form KT similar to the globally coupled case in Sec. III. So, KT is our intrinsic parameter. With the same procedure, the averages of diagonal terms are obtained as Eq. (4.8b).

Now let us turn to the calculation of higher moments of off-diagonal elements A_{jk}. In particular, we have to calculate the mean square $\langle A_{jk}^2\rangle$, i.e., the square of the matrix element and not the matrix element of the squared matrix, to obtain the function $\tilde{J}(KT,p)$. For large N, the most dominant contribution in the coefficient of $O(T^m)$ in the expansion of $\langle A_{jk}^2\rangle$ turns out to be proportional to a_1^m $(m\geqslant 3)$. Thus we can estimate up to $O(N^{-2})$, and find

$$\langle A_{jk}^2\rangle = T^2a_2+T^3\frac{2}{2!}Na_1^3 + T^4\left(\frac{1}{(2!)^2}+\frac{2}{3!}\right)N^2a_1^4+\cdots+O(N^{-3}).$$

Taking the thermodynamic limits, we consequently find Eq. (4.8c) using the same assumption made above. Similarly, other higher moments are obtained as Eq. (4.8d) and so on. The calculation of higher moments of diagonal elements is not necessary for the present purpose.

The calculation of moments of B_{jk} can be performed much more easily, since the matrix in the exponential is diagonal. The averaged off-diagonal part $\langle B_{jk}\rangle$ vanishes and the diagonal part $\langle B_{jj}\rangle$ is readily given by

$$\langle B_{jj}\rangle = 1+(-T)Na_1+\frac{1}{2!}(-T)^2N^2a_1^2+\frac{1}{3!}(-T)^3N^3a_1^3 + \frac{1}{4!}(-T)^4N^4a_1^4+\cdots+O(N^{-1}).$$

Summing up this expansion leads approximately to (4.9) in the thermodynamic limit. Note that the factor N results from the number of matrix elements D_{jk} in the diagonal $\hat{D}_{jk}$. After all, the averaged matrix B is neither more nor less than the unit matrix multiplied by a scalar. This simplicity gives (4.9) as the higher moments of B_{jk}, which means no deviation from the corresponding power of its mean value. All moments of off-diagonal elements vanish.

[1] Y. Kuramoto, *Chemical Oscillators, Waves, and Turbulence* (Springer, Berlin, 1984).
[2] M. C. Cross and P. C. Hohenberg, Rev. Mod. Phys. **65**, 854 (1993).
[3] S. H. Strogatz, *Nonlinear Dynamics and Chaos: With Applications to Physics, Biology, Chemistry, and Engineering* (Addison-Wesley, Reading, MA, 1994).
[4] R. Eckhorn *et al.*, Biol. Cybern. **60**, 121 (1988).
[5] C. M. Gray, P. König, A. K. Engel, and W. Singer, Nature (London) **338**, 334 (1989).
[6] E. Vaadia *et al.*, Nature (London) **373**, 515 (1995).
[7] Y. Kuramoto, in *Proceedings of the Symposium on Mathemati-*

cal Problems in Theoretical Physics, edited by H. Araki, Lecture Notes in Physics Vol. 39 (Springer, New York, 1975).
[8] V. Hakim and W.-J. Rappel, Phys. Rev. A **46**, R7347 (1992); Europhys. Lett. **27**, 637 (1994).
[9] N. Nakagawa and Y. Kuramoto, Prog. Theor. Phys. **89**, 313 (1993); Physica D **75**, 74 (1994); **80**, 307 (1995).
[10] P. C. Matthews and S. H. Strogatz, Phys. Rev. Lett. **65**, 1701 (1990); P. C. Matthews, R. E. Mirollo, and S. H. Strogatz, Physica D **52**, 293 (1991).
[11] Y. Kuramoto and I. Nishikawa, J. Stat. Phys. **49**, 569 (1987).
[12] H. Daido, J. Stat. Phys. **60**, 753 (1990); Physica D **91**, 24 (1996).
[13] S. H. Strogatz and R. E. Mirollo, J. Stat. Phys. **63**, 613 (1991).
[14] K. Okuda, Physica D **63**, 424 (1993).
[15] S. Watanabe and S. H. Strogatz, Phys. Rev. Lett. **70**, 2391 (1993).
[16] H. Daido, Prog. Theor. Phys. **75**, 1460 (1986); J. Phys. A **20**, L629 (1987).
[17] K. Kaneko, Physica D **54**, 5 (1991).
[18] H. Daido, Prog. Theor. Phys. **77**, 622 (1987).
[19] H. Daido, Phys. Rev. Lett. **68**, 1073 (1992).
[20] K. Satoh, J. Phys. Soc. Jpn. **58**, 2010 (1989).
[21] L. L. Bonilla, C. J. Pérez Vicente, and J. M. Rubí, J. Stat. Phys. **70**, 921 (1993).
[22] Y. Kuramoto, Prog. Theor. Phys. Suppl. **79**, 719 (1981).
[23] A. J. Noest, in *Proceedings of the IEEE Conference on Neural Information Processing Systems, Neural and Synthetic*, Denver, 1987, edited by D. Z. Anderson (AIP, New York, 1987); Europhys. Lett. **6**, 469 (1988); Phys. Rev. A **38**, R2196 (1988).
[24] K. Okuda (unpublished).
[25] T. Yamada and H. Fujisaka, Prog. Theor. Phys. **70**, 1240 (1983); **72**, 885 (1984).
[26] It is easy to observe that Eq. (2.5) is obtained by integrating the coupled kicked oscillator system, $\dot{W}^{(j)}=[f_T(W^{(j)},W^{(j)*})-W^{(j)}]\Sigma_n\delta(t-nT)+\mathcal{D}W^{(j)}$.
[27] D. J. Amit, *Modeling Brain Function* (Cambridge University Press, Cambridge, 1989).
[28] W. S. McCullock and W. A. Pitts, Bull. Math. Biophys. **5**, 115 (1943).
[29] D. Sherrington and S. Kirkpatrick, Phys. Rev. Lett. **35**, 1792 (1975); S. Kirkpatrick and D. Sherrington, Phys. Rev. B **17**, 4384 (1978).
[30] Precisely, the phase diagram discussed in [29] is spanned on the $(\beta^{-1}/\tilde{J},\tilde{J}_0/\tilde{J})$ plane. (Here, we use β^{-1} as the temperature so as not to confuse with the discrete time step T.) But, there is no quantity corresponding to the thermal noise in our model. Thus, when we observe the phase transition in their phase space $(\beta^{-1}/\tilde{J},\tilde{J}_0/\tilde{J})$, only the value of $\tilde{J}_0/\tilde{J}$ on a line $\beta^{-1}=0$ is meaningful.
[31] N. G. van Kampen, *Stochastic Process in Physics and Chemistry* (North-Holland, Amsterdam, 1981).
[32] The concept ''oscillator glass'' was first introduced by Daido [18] in his coupled oscillator system with the frustrated interactions leading to in-phase or anti-phase oscillators. The present disordered phase is an example of oscillator glass.
[33] In general, the deterministic noise, resulted from the absence of Liapunov function, enables the system to escape from local attractors. That explains the relaxation to UPD state for $C_2\neq 0$.
[34] M. Gabay and G. Toulouse, Phys. Rev. Lett. **47**, 201 (1981).
[35] D. M. Cragg, D. Sherrington, and M. Gabay, Phys. Rev. Lett. **49**, 158 (1982).
[36] This discussion stands for the phase transition on a line $\beta^{-1}=0$ as mentioned in [30].
[37] H. Sakaguchi, Phys. Lett. A **174**, 289 (1993).
[38] T. Aoyagi, Phys. Rev. Lett. **74**, 4075 (1995).
[39] S. Miyashita and H. Shiba, J. Phys. Soc. Jpn. **53**, 1145 (1984).